

Constraint-Based Causal Structure Learning from Undersampled Graphs

Mohammadsajad Abavisani^{1,2*}, David Danks³ and Sergey Plis^{2,4}

¹Georgia Institute of Technology

²Center for Translational Research in Neuroimaging and Data Science (TReNDS)

³University of California, San Diego

⁴Georgia State University

s.abavisani@gatech.edu, ddanks@ucsd.edu, s.m.plis@gmail.com

Abstract

Graphical structures estimated by causal learning algorithms from time series data can provide highly misleading causal information if the causal timescale of the generating process fails to match the measurement timescale of the data. Although this problem has been recently recognized, practitioners have limited resources to respond to it, and so must continue using models that they know are likely misleading. Existing methods either (a) require that the difference between causal and measurement timescales is known; or (b) can handle only very small number of random variables when the timescale difference is unknown; or (c) apply to only pairs of variables, though with fewer assumptions about prior knowledge; or (d) return impractically too many solutions. This paper addresses all four challenges. We combine constraint programming with both theoretical insights into the problem structure and prior information about admissible causal interactions. The resulting system provides a practical approach that scales to significantly larger sets (> 100) of random variables, does not require precise knowledge of the timescale difference, supports edge misidentification and parametric connection strengths, and can provide the optimum choice among many possible solutions. The cumulative impact of these improvements is gain of multiple orders of magnitude in speed and informativeness.

1 Introduction

Dynamic causal systems play a pivotal role in modeling many real world systems in economics, education, climatology, and neuroscience. Given a sufficiently accurate system model using a causal graph over random variables, it is feasible to predict behavior of, and more generally understand, these systems. In practice, however, it can be quite difficult to specify or learn an accurate causal model of a dynamic system for both statistical and theoretical reasons.

One particular challenge arises when data are not measured at the speed of the underlying causal connections. For example, fMRI scanning of the brain measures bloodflow and oxygen level changes in different brain regions as a result of neural activity (and so increased oxygen consumption level); that is, fMRI provides data about an important dynamical system. However, this sampling takes place (at most) every second while the brain’s actual dynamics is known to occur faster [Oram and Perrett, 1992], though we do not know how much faster. And in general, when the measurement timescale is significantly slower than the causal timescale, then learning can output arbitrarily incorrect causal information (i.e., edge direction or commission/omission error for any pair of variables).

In this paper, we consider the problem of learning the causal structure at the *causal* timescale from data collected at the *measurement* timescale. This challenge has received significant attention in recent years, but all current algorithms have significant limitations (see section 2) that make them unusable for many real-world scientific challenges. The current algorithms show that causal learning from undersampled data is theoretically possible, but they provide little help for its practical possibility. Our goal here is to develop practically useful and effective algorithms—e.g., that could be applied to neuroimaging datasets—for learning causal timescale structure from undersampled data.

2 Related Works And Notation

A directed dynamic causal model is a generalization of “regular” causal models: graph \mathbf{G} includes distinct nodes for random variables \mathbf{V} at both the current timestep t , and also each previous timestep in which there is a direct cause of some current variable of \mathbf{V} . We assume that the “true” underlying causal structure is first-order Markov: the only direct causes of variables at t are those at $t - 1$.¹ \mathbf{G} is thus over $2\mathbf{V}$, and the only permissible edges are $V_i^{t-1} \rightarrow V_j^t$, where possibly $i = j$. The quantitative component of the dynamic causal model is thus fully specified by the relevant conditional probabilities: $P(\mathbf{V}^t | \mathbf{V}^{t-1})$. We assume that these conditional probabilities are stationary over time, but the marginal $P(\mathbf{V}^t)$ need not be stationary.

¹This assumption is relatively weak since we do *not* assume that we measure at this “true” causal timescale.

*s.abavisani@gatech.edu

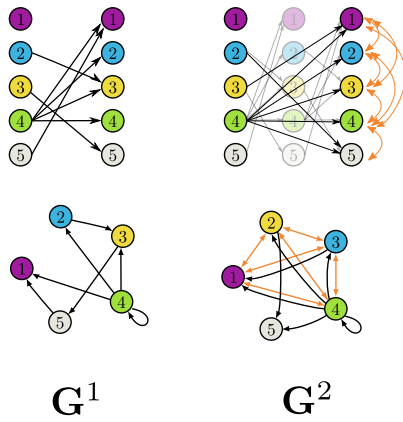


Figure 1: Example of causal graph (left) and effect of undersampling at rate 2 (right)

Denote the timepoints of the underlying causal structure as $\{t^0, t^1, t^2, \dots, t^k, \dots\}$. The data are said to be *undersampled at rate u* if measurements occur at $\{t^0, t^u, t^{2u}, \dots, t^{ku}, \dots\}$. The true causal graph (i.e., undersampled at rate 1) is \mathbf{G}^1 and that same graph undersampled at rate u is \mathbf{G}^u . To determine the implied \mathbf{G} at other timescales, the graph is first “unrolled” by adding instantiations of \mathbf{G}^1 at previous and future timesteps, where \mathbf{V}^{t-2} bear the same causal relationships to \mathbf{V}^{t-1} that \mathbf{V}^{t-1} bear to \mathbf{V}^t , and so forth. In this unrolled (time-indexed by t) graph, all \mathbf{V} at intermediate timesteps are not measured; this lack of measurement is equivalent to marginalizing out (the variables in) those timesteps to yield \mathbf{G}^u .

Marginalizing in this context thus means that: (1) $V_i^{t-u} \rightarrow V_j^t$ in \mathbf{G}^u iff there is a directed path from V_i^{t-u} to V_j^t in \mathbf{G}^1 ; and (2) $V_i^t \leftrightarrow V_j^t$ in \mathbf{G}^u iff there is some V_k^{t-s} with $s < k$ and directed paths from V_k^{t-s} to V_i^t , and also to V_j^t in \mathbf{G}^1 (i.e., an unobserved common cause fewer than u timesteps back). [Danks and Plis, 2013] provided a series of theorems and corollaries that characterize the precise graphical changes under repeated application of the undersample “operator.”

For convenience, we will normally use condensed graphs over only \mathbf{V} , where temporal information is implicitly encoded in the edges. In particular, a condensed graph version of unrolled graph \mathbf{G}^u has $V_i \rightarrow V_j$ iff $V_i^{t-u} \rightarrow V_j^t$ in \mathbf{G}^u ; and $V_i \leftrightarrow V_j$ iff $V_i^t \leftrightarrow V_j^t$ in \mathbf{G}^u . See Figure 1 for example graphs and operations: the unrolled graph (and condensed version) on the left becomes the unrolled graph (and condensed version) on the right if we undersample at rate 2.

Given this framework, the overall causal learning challenge can now be restated as: given \mathbf{G}^u but not u (or dataset \mathbf{D} at unknown undersample rate), what is the set of possible \mathbf{G}^1 ? There will often be many, perhaps infinitely many, possible \mathbf{G}^1 for a given \mathbf{G}^u . At the same time, there will often be only a small number of possible \mathbf{G}^1 , in which case we can avoid using the (possibly misleading) \mathbf{G}^u . One key notion that will be important in understanding learning complexity is a (maximal) *strongly connected component* (SCC): sets of nodes such that there is a path from every node to every other.

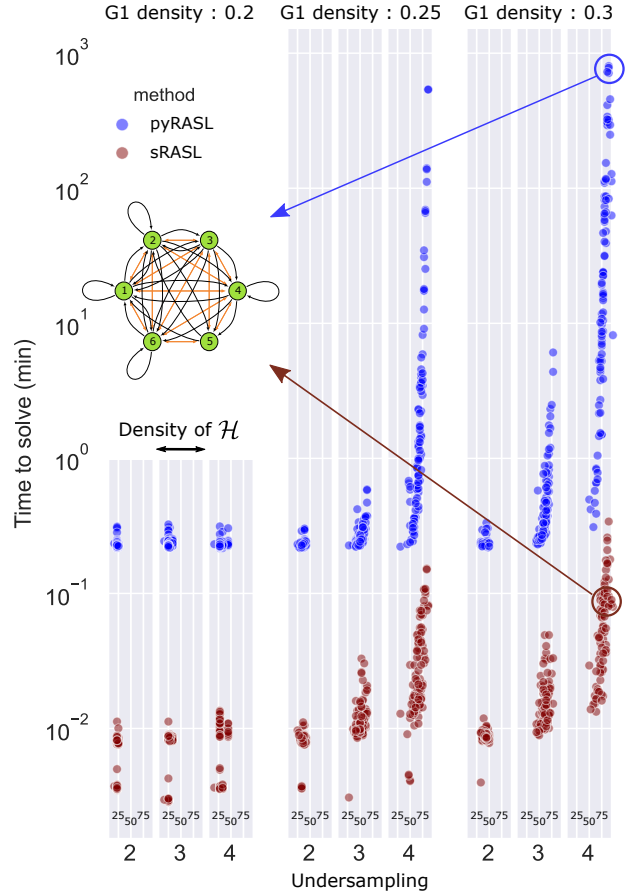


Figure 2: Comparison of presented sRASL method (red) with previous state-of-the-art method (blue).

Multiple algorithms have been developed to learn (a set of) \mathbf{G}^1 given \mathcal{H} (the causal graph inferred from data \mathbf{D}), each with its own distinctive shortcomings. An obvious brute-force algorithm is: for all \mathbf{G}^1 , compute the corresponding \mathbf{G}^u for all u , and then output all \mathbf{G}^1 such that there is some u for which $\mathbf{G}^u = \mathcal{H}$. However, this algorithm will be computationally intractable for any reasonable n , as there are 2^{n^2} possible \mathbf{G}^1 and u can (in theory) be arbitrarily large.

Mesochronal Structure Learning (MSL) [Plis et al., 2015b] aims to exactly determine the set of \mathbf{G}^1 . Every edge in \mathbf{G}^u corresponds to one or more paths of length u in \mathbf{G}^1 , and so \mathbf{G}^1 can be constructed if we can identify $u - 1$ nodes along every edge in \mathbf{G}^u . MSL searches the state space of possible identifications in a Depth-First Search (DFS) manner. Every identification yields a \mathbf{G}^1 ; the corresponding \mathbf{G}^u can then be efficiently calculated. If the calculated \mathbf{G}^u is the same as the one acquired from data, then this \mathbf{G}^1 is added to the output *equivalence class*. Otherwise, the search continues. In addition, MSL backtracks in the DFS whenever the transition from \mathbf{G}^1 to \mathbf{G}^u results in an edge that is not present in measured \mathbf{G}^u from data. In this case, the candidate \mathbf{G}^1 and all its supergraphs will not be considered any further.

Although [Plis et al., 2015b] showed that the concept that causal inference from undersampled data is feasible, MSL is

```

1  %( * input graph edge specifications here * e.g.:
   hdirected(1,5,1) ... )
2  %( * input graph SCC specifications here * e.g.:
   sccsize(0, 5). scc(1, 0) ...)
3  #const n = 10, maxu = 20
4  node(1..n).
5  1 {u(1..maxu, 1)} 1.
6  :- edge1(X,Y), scc(X, K), scc(Y, L), K != L,
   sccsize(L, Z), Z > 1, not dag(K, L).
7  {edge1(X,Y)} :- node(X), node(Y).
8  directed(X, Y, 1) :- edge1(X, Y).
9  directed(X, Y, L) :- directed(X, Z, L-1),
   edge1(Z, Y), L <= U, u(U, _).
10
11 bidirected(X, Y, U) :- directed(Z, X, L),
   directed(Z, Y, L), node(X;Y;Z), X < Y, L < U,
   u(U, _).
12 :- directed(X, Y, L), not hdirected(X, Y, K),
   node(X;Y), u(L, K).
13 :- bidirected(X, Y, L), not hbidirected(X, Y, K),
   node(X;Y), u(L, K), X < Y.
14 :- not directed(X, Y, L), hdirected(X, Y, K),
   node(X;Y), u(L, K).
15 :- not bidirected(X, Y, L), hbidirected(X, Y, K),
   node(X;Y), u(L, K), X < Y.

```

Listing 1: Clingo code for sRASL

computationally intractable on even moderate-sized graphs. [Hyttinen *et al.*, 2017] used the implied constraints to develop an Answer Set Programming (ASP) method that formulated this causal inference challenge as a rule-based constraint satisfaction problem. In essence, the algorithm takes as input the measured causal graph \mathcal{H} , determines the set of implied constraints on \mathbf{G}^1 , and then uses the general-purpose Answer Set Solver *Clingo* [Gebser *et al.*, 2011] to determine the set of possible \mathbf{G}^1 orders of magnitude faster than MSL [Plis *et al.*, 2015b].

Although the method in [Hyttinen *et al.*, 2017] is significantly faster, it requires us to specify the undersampling rate u (or else run the method sequentially for all possible u , thereby losing much of the computational advantage). In contrast, the *Rate-Agnostic (Causal) Structure Learning (RASL)* approach [Plis *et al.*, 2015a] makes no such assumption. Rather, [Plis *et al.*, 2015a] developed three different constructive and iterative RASL algorithms to find the \mathbf{G}^1 equivalence class without knowing (or surveying all possible) u . These algorithms achieve faster performance by using two key stopping rules for given \mathbf{G}^1 : (1) if some \mathbf{G}^k has previously been seen by the algorithm, then further undersampling of \mathbf{G}^1 will not produce novel graphs; and (2) if \mathbf{G}^k is not an edge-subset of \mathcal{H} for all k , then do not consider any edge-superset of \mathbf{G}^1 [Plis *et al.*, 2015a]. Despite improvements, RASL still faces memory and run-time constraints for even moderate numbers of nodes.

In this paper, we develop *sRASL*, a novel algorithm that integrates the best features of both ASP solvers and RASL to obtain a rate-agnostic method that is also able to process substantially larger graphs. By encoding the problem in a declarative language [Fahland *et al.*, 2009], we increased the solution speed by up to three orders of magnitude, thereby enabling us to solve causal inference from undersampling prob-

```

1  :- not directed(X, Y, L), hdirected(X, Y, W,
   K), node(X;Y), u(L, K). [W@1,X,Y]
2  :- not bidirected(X, Y, L), hbidirected(X, Y,
   W, K), node(X;Y), u(L, K), X < Y. [W@1,X,Y]
3  :- directed(X, Y, L), no_hdirected(X, Y, W, K),
   node(X;Y), u(L, K). [W@1,X,Y]
4  :- bidirected(X, Y, L), no_hbidirected(X, Y, W,
   K), node(X;Y), u(L, K), X < Y. [W@1,X,Y]

```

Listing 2: Integrity constraints for turning sRASL algorithm into an optimization problem when they replace lines 12 through 15 in Listing 1

lems involving over 100 nodes. For example, Figure 2 shows a comparison of our method (red) with the previously-fastest method (blue) on the same graphs. A graph that took nearly 1000 minutes to compute with RASL [Plis *et al.*, 2015a] was finished in 6 seconds with our new approach.

3 Approach

This section describes the sRASL algorithm. The input is a (potentially) undersampled graph \mathcal{H} that could be learned from data \mathbf{D} , expert domain knowledge, or some other source; sRASL is agnostic about the source of the input graph [Danks and Plis, 2019]. In the ideal case, the output is the complete equivalence class of all \mathbf{G}^1 such that undersampling of \mathbf{G}^1 would yield \mathcal{H} . In practice, statistical noise or other errors can result in \mathcal{H} for which there is *no* \mathbf{G}^1 such that $\mathbf{G}^u = \mathcal{H}$. In such cases, sRASL finds the set of \mathbf{G}^1 that are, for some, also estimated, undersample rate, closest to \mathcal{H} . To achieve that we need to replace the exact integrity constraints of Listing 1 with optimization formulation of Listing 2. In this case, we are able to specify the importance or weight of each edge in the measured graph \mathcal{H} , represented by \mathbf{W} in Listing 2. See [Gebser *et al.*, 2011] for details of optimization in *clingo*.

This algorithm is able to leverage high-level structure within \mathcal{H} . The nodes in a condensed graph can be partitioned into SCCs, where the connections between SCCs must themselves form a directed acyclic graph. That is, let X, Y be in SCCs \mathbf{A}, \mathbf{B} respectively; if $X \rightarrow Y$, then there cannot be an edge from any $B \in \mathbf{B}$ to any $A \in \mathbf{A}$. If there were such an edge, then there would be a path from any node in \mathbf{A} to any node in \mathbf{B} and vice versa, so $\mathbf{A} \cup \mathbf{B}$ would be a single SCC.

Moreover, under a weak additional assumption,² SCC membership is preserved under undersampling. Structural features thus potentially provide many additional constraints beyond the obvious ones. In particular, if \mathcal{H} has a roughly modular structure—that is, the SCCs are not too large—then sRASL generates many more constraints than the algorithm of [Hyttinen *et al.*, 2017].

Listing 1 shows the Clingo code for the most comprehensive version of sRASL. In the first line, we input the first-order graph-specific specification of \mathcal{H} (e.g., the edge $1 \rightarrow 10$ translates to *hdirected*(1, 10)). Line 2 encodes the second-order structure of \mathcal{H} , including the partition of \mathbf{V} into SCCs.

²Greatest common divisor of cycle lengths within each SCC is 1.

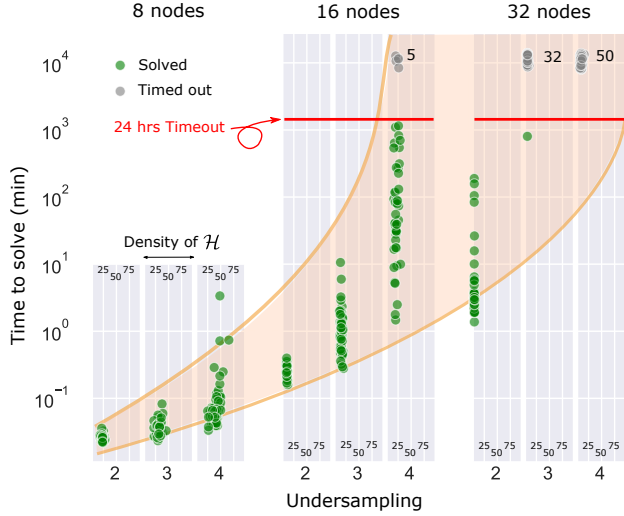


Figure 3: Time behavior of graphs of size 8, 16 and 32. The time out for this experiment indicated by the red line was 24 hours. *Green* dots represent graphs that has been computed within the 24-hours window. *Gray* represent graphs that could not be fully computed within 24-hours window.

These predicates and basic descriptive information are added to the Clingo code (lines 3, 4, 5) in an automated way.³

This implementation of sRASL allows the user to specify a maximum undersampling rate to consider (maxu on line 3). [Plis *et al.*, 2015a, Theorem 3.1] provides an upper bound for when undersampling could involve informative changes. In practice, the plausible undersampling rate will often be much lower than the theoretical upper bound. Our efforts are primarily directed towards neuroimaging applications, so we here use a maximum undersampling rate of 20. The underlying rate of brain activity is generally thought to be ~ 100 milliseconds and fMRI devices measure approximately every two seconds. Hence, $u = 20$ is a plausible upper bound on undersampling in fMRI studies.⁴

Line 6 adds the additional constraints implied by the acyclicity of between-SCC connections. And lines 7 – 8 ensure that we consider the full space of possible \mathbf{G}^1 . Lines 9 and 10 find paths of length L in the graph (i.e., an edge in \mathbf{G}^L). Line 11 similarly finds bidirected edges in \mathbf{G}^L . Lines 12 – 15 then ensure that sRASL returns only \mathbf{G}^1 for which there exists u such that $\mathbf{G}^u = \mathcal{H}$. If sRASL initially returns the empty set (i.e., there are no suitable \mathbf{G}^1), then sRASL instead finds optimal (though not perfect) outputs (see Section 4.5 for details).

4 Results

In this section, we analyze empirical performances of sRASL in a number of representative simulations.

³The code is available at [retracted for anonimity](#)

⁴Of course, the actual undersample rate could be much lower than 20. Voxels typically contain 8 – 10 layers of neurons, so the “causal timescale of a voxel” could easily be 1000 ms (i.e., $u = 2$).

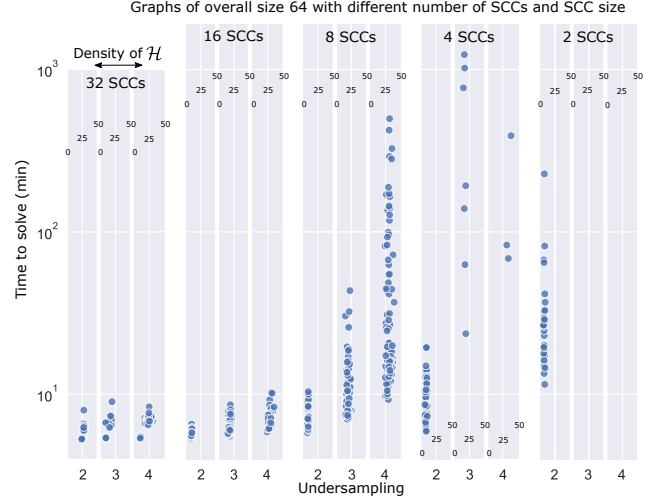


Figure 4: Time behavior of graphs of size 64 with various sub SCC sizes. The time out for this experiment was 24 hours (1440 Minutes).

4.1 Comparing Methods

The goal of this experiment is to compare our proposed method with the existing method and demonstrate its superiority (Figure 2). In this experiment, we have generated 100 6-node SCCs for each of 3 densities in $[0.2, 0.25, 0.3]$ which were then each undersampled by 2, 3 and 4. Each column of Figure 2 consists of graphs of approximately same density, i.e from left to right 20%, 25% and 30%. The size of the graphs in this experiment are chosen as six because that is the maximum number of nodes that the previous state-of-the-art *pyRASL* [Plis *et al.*, 2015a] algorithms could handle in a reasonable time and space.

After obtaining undersampled graphs, the same 100 graphs that have been undersampled are used as the input to each of these two algorithms. After completion, we will save the size of the equivalence class and the time it took to find these solutions. As we can see in Figure 2, our proposed method is three orders of magnitude faster than the previous method.

4.2 Comparing Graph Size

The goal of this experiment is twofold: firstly, we want to show that sRASL is capable of finding equivalence classes for much larger graphs compared to existing methods. As we can see in Figure 3, sRASL can find equivalence classes for graphs that are composed of a single SCC of size 32 nodes within 24 hours. Secondly, we want to demonstrate the effect of the SCC size in a single SCC setting. The choice of a single SCC is motivated by the expected use of our algorithms for scientific analysis of real world systems, which usually, especially in living systems, are modular. Each module consist of strongly interacting parts with a tighter connection and with many feedback loops. These modules connecting together form the overall system. As we can see, the complexity of the problem and, as a result, the time to compute it increases exponentially.

In this experiment, 50 graphs of each size, namely 8, 16

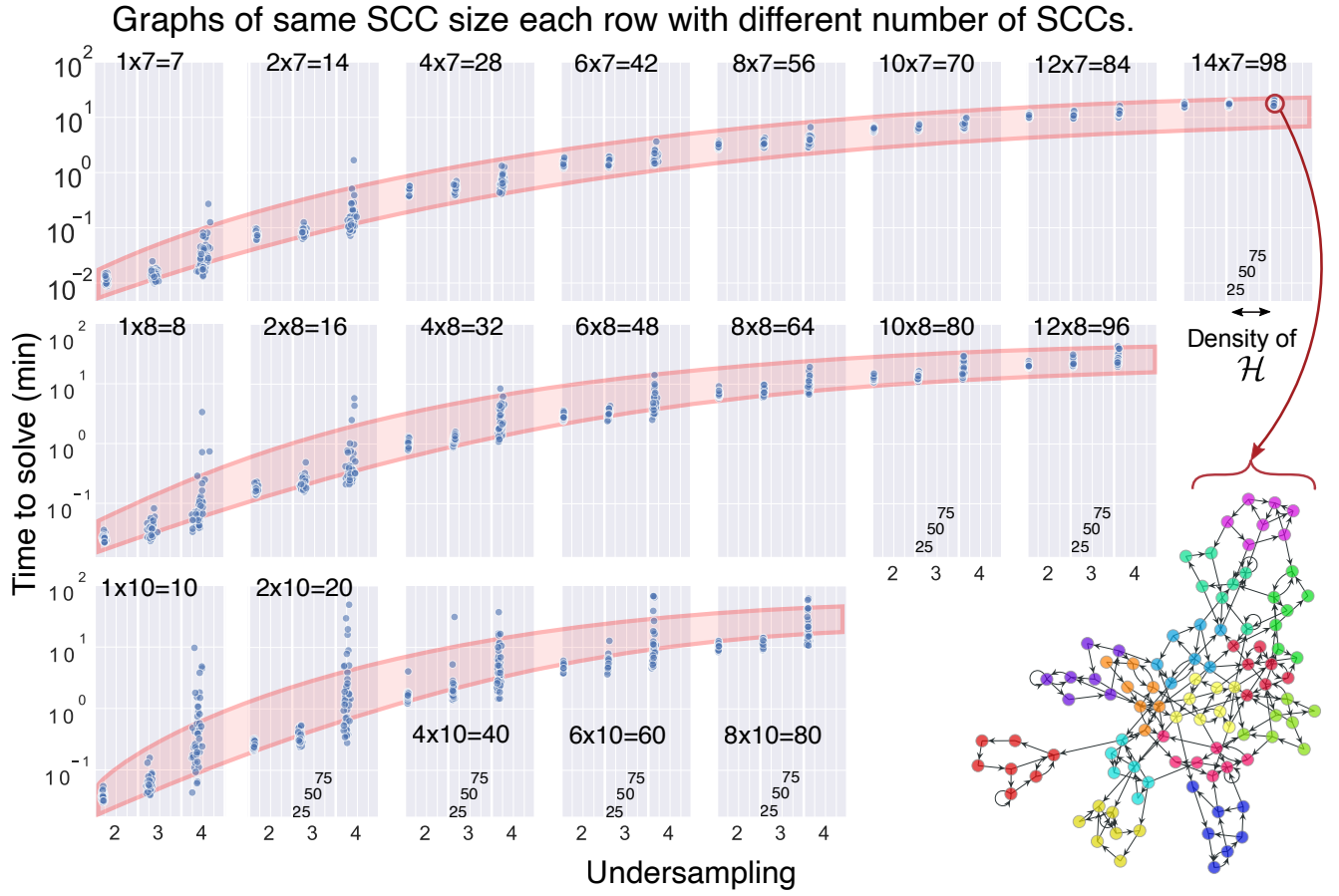


Figure 5: Time behaviour of graphs with the same SCCs sizes but with multiple number of SCCs. Top row graphs of SCC size 7 with 1, 2, ..., 14 number of SCCs. Middle row graphs of SCC size 8. Bottom row graphs of SCC size 10. Bottom right corner is an example of a structured graph with 98 nodes structured as 14 SCCs of size 7. Each color represents one Strongly Connected Component.

and 32 with average degree of 1.4 outgoing edges per node are randomly generated and then undersampled by 2, 3 and 4 and used as input to sRASL.

4.3 Comparing SCC Size

The goal of this experiment is show the performance of sRASL on large, structured graphs. The idea is that in most real-world problems, systems consist smaller sub-sections with feedback loops in each subsection. Therefore, as a graphical model, most realistic graphs are composed of several parts that are interconnected, i.e. SCCs, and then these parts are connected to each other to make one big graphs. In order to simulate this behaviour, this experiment analyzes graphs of size 64 nodes that are constructed of (left to right in Figure 4) 32 SCCs of size 2, 16 SCCs of size 4, 8 SCCs of size 8, 4 SCCs of size 16 and 2 SCCs of size 32.

As we can see from Figure 4, although the total number of nodes is 64 in all instances, the SCC size has a pivotal role in the complexity of the problem as computation period grows super-exponentially by increased SCC size. For each column in Figure 4, 50 random graphs have been computed. As we move towards the right columns, the time complexity increases and more and more of the graphs were not able

to compute the equivalent class before the 24-hours timeout (Less blue dots).

In this experiment, sRASL takes advantage of the structured graph by considering each SCC separately, and thus computes the equivalent class much faster. Had it been only looking at the 64 nodes graph as a whole, we would have not seen any difference between time complexity of columns in Figure 4. The structure of the graphs in here consists of several SCCs with average degree 1.4 outgoing edges connected together with a DAG of average degree 2. Edges of the DAG represent path from one SCC to another. However, in the graph, this path may be realized randomly with several edges from origin SCC to the destination SCC.

4.4 Comparing Graph Size With Constant SCC Size

The goal of this experiment is show that the key factor in complexity of solving graphs is by large the size of the SCCs in the structured graph (Figure 5). Based on empirical evidence, by keeping the size of the SCCs constant and adding several of these fix-sized SCCs to the graph, time complexity increases but with a lower rate than that of increasing the

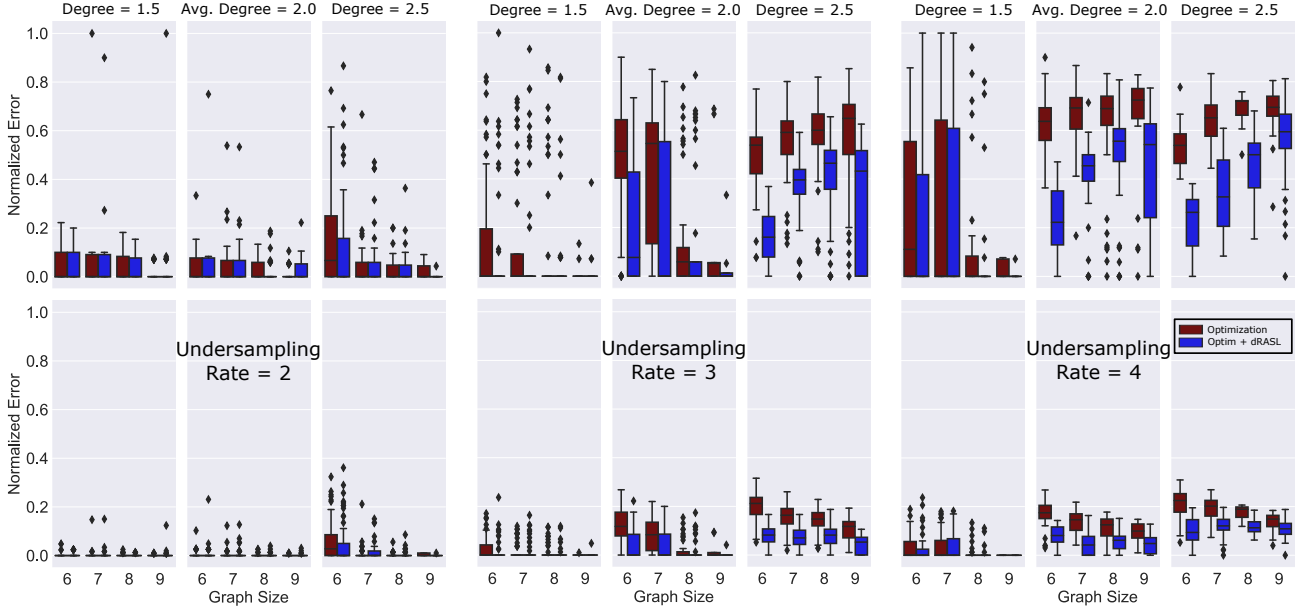


Figure 6: The omission (top) and commission (bottom) error of different graph sizes and undersampling of two, three and four from left to right.

SCC sizes. Same as Section 4.3, the graph is structured such that each SCC have an average degree of 1.4 and SCCs are connected with DAG of degree 2.

Based on the several experiments we did in this section on different SCC sizes 7, 8 and 10, by adding one SCC of same size to the graph, the time complexity will grow *linearly*. Whereas, based on evidence from previous sections (see sections 4.2 and 4.3) adding nodes to a graph will increase the time complexity super-exponentially. While the graph illustrated on bottom right corner of Figure 5 has 98 nodes, sRASL can compute the equivalent class of this graph in approximately 20 minutes (Compare this to 17 hours to compute a graph of size 6 with pyRASL).

Given the rate at which we could compute equivalent class of large graphs, we could in theory go to much larger graphs. However, it seems to be a limitation of Clingo language that it can only handle so many atoms. Therefore, in our experiments graphs of size 100 seems to be the limit for Clingo to handle all the predicates. We can consider it a future directions to optimize sRASL to produce fewer predicates.

4.5 Optimization

In this experiment, we use the optimization capability of Clingo. In particular, if there are multiple stable models, Clingo can optimize based on the weights and priorities that we set, and output a single solution with minimum cost function along with an undersampling rate u corresponding to this solution. For this experiment, we first identify \mathcal{H} such that the equivalence class of \mathbf{G}^1 is non-singleton. We then assign weight to the edges of the \mathcal{H} and randomly break one edge from it. We then run sRASL on this “broken” \mathcal{H} to find \mathbf{G}^1 with undersampled \mathbf{G}^u (for some u) that are closest (relative to the edge weights) to \mathcal{H} . As seen in Figure 6 (red bars), except for high undersamplings, sRASL frequently retrieves

the true \mathbf{G}^1 ; that is, sRASL is robust to small errors in \mathcal{H} in many settings.

Another approach to obtain the optimally consistent \mathbf{G}^1 from a broken \mathcal{H} is to first same as before run the optimization and acquire a pair of solution \mathbf{G}_{opt}^1 and undersampling rate u_{opt} . This solution will not be undersampled, i.e. it is in the \mathbf{G}^1 space. From there, we will undersample this solution \mathbf{G}_{opt}^1 by u_{opt} to get \mathbf{G}_{opt}^u . Then \mathbf{G}_{opt}^u is used as the input for the regular sRASL to get the equivalent class. The error then is calculated based on the minimum error among all the \mathbf{G}^1 s in the equivalent class. As we can see from Figure 6 (blue bars), we will always have improvement compared to regular optimization in terms of both commission and omission error.

5 Conclusion And Discussion

Real-world scientific problems frequently involve measurement processes that operate at a different timescale than the causal structure of the system under study. If measurements occur at a slower rate than the causal influences, then causal discovery from those undersampled data can yield highly misleading outputs. Multiple methods have been developed to infer aspects of the underlying causal structure from the undersampled data/graph. However, the assumptions or computational complexities of those algorithms make them unusable for most real-world challenges. In this paper, we have developed and tested sRASL, a novel algorithm that does not suffer from those same limitations. sRASL is suitable for large (100-node) graphs, and does not require the end-user to know the actual undersampling rate. Future research will focus on application of sRASL to actual neuroimaging data, and extensions to situations with multiple measurement modalities.

6 Acknowledgement

This work was supported by NIH R01MH129047 and in part by NSF 2112455, and NIH 2R01EB006841

References

- [Danks and Plis, 2013] David Danks and Sergey Plis. Learning causal structure from undersampled time series. 2013.
- [Danks and Plis, 2019] David Danks and Sergey Plis. Amalgamating evidence of dynamics. *Synthese*, 196(8):3213–3230, 2019.
- [Fahland *et al.*, 2009] Dirk Fahland, Daniel Lübke, Jan Mendling, Hajo Reijers, Barbara Weber, Matthias Weidlich, and Stefan Zugal. Declarative versus imperative process modeling languages: The issue of understandability. In *Enterprise, Business-Process and Information Systems Modeling*, pages 353–366. Springer, 2009.
- [Gebser *et al.*, 2011] Martin Gebser, Benjamin Kaufmann, Roland Kaminski, Max Ostrowski, Torsten Schaub, and Marius Schneider. Potassco: The potsdam answer set solving collection. *Ai Communications*, 24(2):107–124, 2011.
- [Hytinen *et al.*, 2017] Antti Hyttinen, Sergey Plis, Matti Järvisalo, Frederick Eberhardt, and David Danks. A constraint optimization approach to causal discovery from subsampled time series data. *International Journal of Approximate Reasoning*, 90:208–225, 2017.
- [Oram and Perrett, 1992] MW Oram and DI Perrett. Time course of neural responses discriminating different views of the face and head. *Journal of neurophysiology*, 68(1):70–84, 1992.
- [Plis *et al.*, 2015a] Sergey Plis, David Danks, Cynthia Freeman, and Vince Calhoun. Rate-agnostic (causal) structure learning. In *Advances in neural information processing systems*, pages 3303–3311, 2015.
- [Plis *et al.*, 2015b] Sergey Plis, David Danks, and Jianyu Yang. Mesochronal structure learning. In *Uncertainty in artificial intelligence: proceedings of the... conference. Conference on Uncertainty in Artificial Intelligence*, volume 31. NIH Public Access, 2015.